



# Treatment of human pancreatic cancer using combined ultrasound, microbubbles, and gemcitabine: a clinical case study

Spiros Kotopoulos, Georg Dimcevski, Odd Helge Gilja, Dag Hoem, Michiel Postema

## ► To cite this version:

Spiros Kotopoulos, Georg Dimcevski, Odd Helge Gilja, Dag Hoem, Michiel Postema. Treatment of human pancreatic cancer using combined ultrasound, microbubbles, and gemcitabine: a clinical case study. *Medical Physics*, 2013, 40 (7), pp.072902. 10.1118/1.4808149 . hal-03193216

**HAL Id: hal-03193216**

**<https://hal.science/hal-03193216>**

Submitted on 16 Apr 2021

**HAL** is a multi-disciplinary open access archive for the deposit and dissemination of scientific research documents, whether they are published or not. The documents may come from teaching and research institutions in France or abroad, or from public or private research centers.

L'archive ouverte pluridisciplinaire **HAL**, est destinée au dépôt et à la diffusion de documents scientifiques de niveau recherche, publiés ou non, émanant des établissements d'enseignement et de recherche français ou étrangers, des laboratoires publics ou privés.

1    **Treatment of human pancreatic cancer using combined ultrasound,**  
2    **microbubbles and gemcitabine: a clinical case study.**

3    Spiros Kotopoulos<sup>1,2 \*</sup>, Georg Dimcevski<sup>1,3</sup>, Odd Helge Gilja<sup>1,3</sup>, Dag Hoem<sup>4</sup>, Michiel  
4    Postema<sup>2,5</sup>

5    <sup>1</sup> National Centre for Ultrasound in Gastroenterology, Haukeland University Hospital, Bergen,  
6    Norway

7    <sup>2</sup> Department of Physics and Technology, University of Bergen, Bergen, Norway

8    <sup>3</sup> Department of Clinical Medicine, University of Bergen, Bergen, Norway

9    <sup>4</sup> Department of Surgery, Haukeland University Hospital, Bergen, Norway

10    <sup>5</sup> The Michelsen Centre for Industrial Measurement Science and Technology, Bergen,  
11    Norway

12

13    **Abstract**

14    Purpose: The purpose of this study was to investigate the ability and efficacy of  
15    inducing sonoporation in a clinical setting, using commercially available technology,  
16    to increase the patients' quality of life and extend the low ECOG performance grade;  
17    as a result increasing the overall survival in patients with pancreatic adenocarcinoma.

18    Methods: Patients were treated using a customised configuration of a commercial  
19    clinical ultrasound scanner over a time period of 31.5 min following standard  
20    chemotherapy treatment with gemcitabine. SonoVue<sup>®</sup> ultrasound contrast agent was  
21    injected intravascularly during the treatment with the aim to induce sonoporation.

22    Results: Using our custom acoustic settings, our patients were able to undergo an  
23    increased number of treatment cycles; from an average of 9 to 16 cycles when

---

\* Corresponding author email: Spiros.Kotopoulos@uib.no

24 comparing to a historical control group of 80 patients. In two out of five patients  
25 treated, the maximum tumour diameter was temporally decreased to  $80\pm 5\%$  and  
26 permanently to  $70\pm 5\%$  of their original size, whilst the other patients showed reduced  
27 growth.

28 We also explain and characterise the settings and acoustic output obtained from a  
29 commercial clinical scanner used for combined ultrasound microbubble and  
30 chemotherapy treatment.

31 Conclusion: It is possible to combine ultrasound, microbubbles, and chemotherapy in  
32 a clinical setting using commercially available clinical ultrasound scanners to increase  
33 the number of treatment cycles, prolonging the quality of life in patients with  
34 pancreatic adenocarcinoma compared to chemotherapy alone.

## 35 **Purpose**

36 Cancer is the world's second largest cause of death with over 7.6 million deaths a year  
37 (21% of NCD deaths) [1]. There are over 217 000 new cases of pancreatic cancer  
38 worldwide every year [2]. Pancreatic cancer is very difficult to treat due to its  
39 aggressive biology, late diagnosis, the encasement of large blood vessels, and the  
40 presence of metastasis. Hence, surgery is rarely an option. Chemotherapy produces  
41 modest responses but is not curative in this setting, mainly because its use is severely  
42 hampered by toxic effects to vital organs. As a result, the survival is very low. The  
43 mortality of the inoperable patients is 50% within 3 months and 90% within 12  
44 months [3, 4].

45 Sonoporation is a novel method for non-invasive targeted drug and gene delivery [5-  
46 8]. Sonoporation is defined as the transient formation of pores in cell membranes  
47 owing to ultrasound or a combination of ultrasound and microbubbles. These pores  
48 range in size from several nanometres to several micrometres [9-12], allowing for  
49 increased drug uptake in highly targeted regions [13-15].

50 The acoustic parameters used for sonoporation showing increased cellular uptake of  
51 chemotherapeutics and genes vary from low-intensity diagnostic ultrasound  
52 (Mechanical Index (MI)  $< 0.3$ ) [16-29] to high-intensity diagnostic ultrasound (MI  $>$   
53 1.0) [9, 30-34]. Throughout literature, the acoustic settings used to induce  
54 sonoporation vary drastically, with a broad range of these settings showing improved  
55 drug and gene delivery. Several studies also show the effect of clinical diagnostic  
56 ultrasound in standard colour-Doppler and B-mode imaging on cellular uptake [19,  
57 20]. These studies, which made use of clinical diagnostic scanners, concluded that a  
58 larger duty cycle was necessary to increase the effect of sonoporation. It has been

59 shown that the ideal settings to induce sonoporation are when shock-waves were not  
60 present, in order to sustain the microbubbles, and when the duty cycle is long enough,  
61 to excite the microbubbles in the targeted area without heating the surrounding tissue  
62 [16]. Furthermore, higher intensities correlating to cavitation and jetting result in  
63 increased cell death due to mechanical damage instead of (transient) sonoporation [33,  
64 35-37]. As a result, there is no consensus on the exact ultrasound settings to be used  
65 for sonoporation [38]. For this reason we aimed to use settings that matched our  
66 previous *in-vitro* and *in-vivo* work as much as possible, *i.e.*, an *in-situ* MI=0.2,  
67 maximum duty cycle, and minimum shockwave generation in order to preserve the  
68 microbubbles [7, 8, 23].

69 To date, all sonoporation experiments have been done either *in vitro* or in animal  
70 models, hence the effect of sonoporation in humans is not truly known yet.

71 Ultrasound has been used as a tool in the clinic for many years, especially in  
72 transabdominal imaging. Specifically, the pancreas can easily be imaged  
73 ultrasonically [39]. In clinical ultrasonic imaging, ultrasound is combined with so-  
74 called ultrasound contrast agents to locate tumours [40, 41]. These agents consist of  
75 gas microbubbles encapsulated by elastic shells [42]. Using a clinical diagnostic  
76 scanner for combined imaging and treatment allows for precise acoustic field  
77 alignment ensuring that the correct ultrasound intensity reaches the target area.

78 In this study, we worked towards optimising the ultrasonic settings for invoking  
79 sonoporation in the target region of a pancreatic tumour using a common commercial  
80 clinical ultrasound scanner without physical modifications.

81

## 82    **Methods**

83    A clinical scanner was calibrated in a degassed water bath in order to map the beam  
84    profile and optimise the acoustic settings. After the chemotherapeutic dose was  
85    delivered, the clinical probe was positioned aiming directly at the pancreatic tumour  
86    and locked in place for 31.5 minutes. The probe was attached to a ball joint and was  
87    positioned near the upper abdomen. Stomach and intestine were avoided in all cases  
88    to ensure propagation only through soft tissue, to ensure delivery of the aimed  
89    ultrasound intensity at the desired area. Once the tumour was located the probe  
90    orientation was fine-tuned in order to locate the largest slice of the tumour and as  
91    much vasculature as possible, *i.e.*, the feeding vessels. The probe was then locked in  
92    position until the completion of the treatment. The natural breathing motion aided the  
93    treatment as the ultrasound slice gently oscillated through the tumour. By visualising  
94    the vasculature and tumour it could be ensured that the microbubbles were being  
95    sonicated at the target. These vessels were then used as a reference point for future  
96    treatments. Nine doses of ultrasound contrast agent were intravenously injected over  
97    this time period to enhance the sonoporation effect. To evaluate the efficacy of the  
98    combined treatment we compared the amount of chemotherapy cycles the patient was  
99    able to receive. Furthermore, the tumour size was measured over the course of the  
100    treatment cycles to monitor and compare the tumour growth.

101

### 102    **Ultrasound scanner configuration**

103

104    A GE LOGIQ 9 ultrasound scanner (GE Healthcare, Waukesha, WI) combined with a  
105    4C curvilinear probe (GE Healthcare) was used for both diagnosis and therapy.

To calibrate and program the diagnostic scanner for the optimised therapeutic settings the probe was locked in position in a custom-made 250-L 3D scanning tank, containing degassed water. A calibrated HGL-200 bullet-type hydrophone (Onda, Sunnyvale, CA) connected to a WaveJet 354a oscilloscope (Teledyne LeCroy SA, Geneva, Switzerland) was used to measure the acoustic signal. The scanning tank had a spatial resolution of 0.4  $\mu\text{m}$ . For the calibration a 200- $\mu\text{m}$  resolution was used. AQUASONIC® ultrasound transmission gel (Parker Laboratories, Fairfield, NJ) was placed on the transducer transmission surface and the probe was subsequently covered using a latex ultrasound probe cover (Sheathing Technologies, Inc., Morgan Hill, CA) prior to submersion. The diagnostic scanner settings were modified in order to achieve a maximum duty cycle without completely degrading the image quality, in addition to having a linear acoustic signal. We aimed for minimal acoustic shockwaves and harmonics minimising potential cavitation. The absence of nonlinear content was verified by visualising the temporal extent of the pulses and performing a Fast Fourier Transform (FFT) [43]. Multiple focal depths (from 2.8 cm to 8.4 cm) and different settings (varying gain, changing window size, etc.) were evaluated to ensure similar acoustic conditions in all cases. To calculate the *in-situ* acoustic pressures and intensities, the *in-water* values were derated by 0.3 dB/MHz/cm, an approximation of soft tissue attenuation in accordance to FDA and IEC guidelines [44, 45]. The attenuation factor of 0.3 dB/MHz/cm is only valid for soft tissue. Hence, this calibration was representative for our clinical positioning for targeting the pancreas.

Table 1 shows the ultrasound scanner settings used to perform the simultaneous observation and treatment of the pancreatic tumours. Skilled clinical sonographers were called upon to judge the image quality. As there are variations between patients,

such as tumour depth and tissue attenuation, certain settings had to be adjusted to ensure the correct ultrasound intensity reached the required area whilst maintaining the image quality. The settings that were varied are labelled as *Patient-dependent*. The three settings that were adjusted prior to treatment were: the focal depth, image depth, and gain. The focal and image depths were adjusted in order to visualise and position the acoustic focus directly in the middle of the tumour. By doing so we could ensure that the acoustic conditions the tumour received was as similar as possible in all patients. The gain is only applied after the received signal, hence it did not affect the acoustic output. The gain simply allowed for a brighter image. Once the probe was locked in position and the tumour was “targeted”, no changes to the ultrasonic conditions were made.

	B-mode	Contrast mode			
Parameter	Value		Unit	Description	Variability
MI	0.4	0.4		Mechanical Index	None
TIs	0.0	0.0		Thermal Index of soft tissue	None
Freq	4.0	4.0	MHz	Centre Receive frequency	None
AO	1	36	%	Normalised acoustic output	None
FR	4	4	fps	Frame rate	None
Gn	30-45	30-45	dB	Gain	Patient-dependent
S/A	3/3	2/0		Synthetic Aperture	None
Map	F/0	2/0		Colour map	None
F	5.2-6.8	5.2-6.8	cm	Focal depth	Patient-dependent
D	10-15	10-15	cm	Image Depth	Patient-dependent
DR	66	66	dB	Dynamic Range	None
SRI HD	3	3		Image smoothing	None
Grey Map	F/0	H		Image colour maps	None



Trig	-0.25	-	s	Trigger delay	None
Tint Map	D	-		Image colour maps	None
Trig	-	0-1		Image triggering	None
TAD	-	on		True Agent Detection	None
F.Average	-	3	frames	Frame averaging	None

**Table 1:** Parameters as indicated on a GE LOGIQ 9 clinical ultrasound scanner.

The settings chosen resulted in acoustic conditions shown in Table 2 and beam profiles shown in Figure 1.

	Centre frequency (MHz)	Duty cycle (%)	Mechanical Index	Acoustic power $I_{SATA}$ (mW/cm <sup>2</sup> )	Peak peak-negative acoustic pressure (MPa)
<i>in-water</i> values at 6.7 cm depth	1.9	1 (4 cycles every 0.21 ms)	0.49	0.59	0.41
Derated <i>in-situ</i> values at 6.7 cm depth	1.9	1 (4 cycles every 0.21 ms)	0.20	0.25	0.27

**Table 2:** Acoustic conditions generated by the 4C probe for sonoporation *in-water* and derated for *in-situ* values [44, 45].

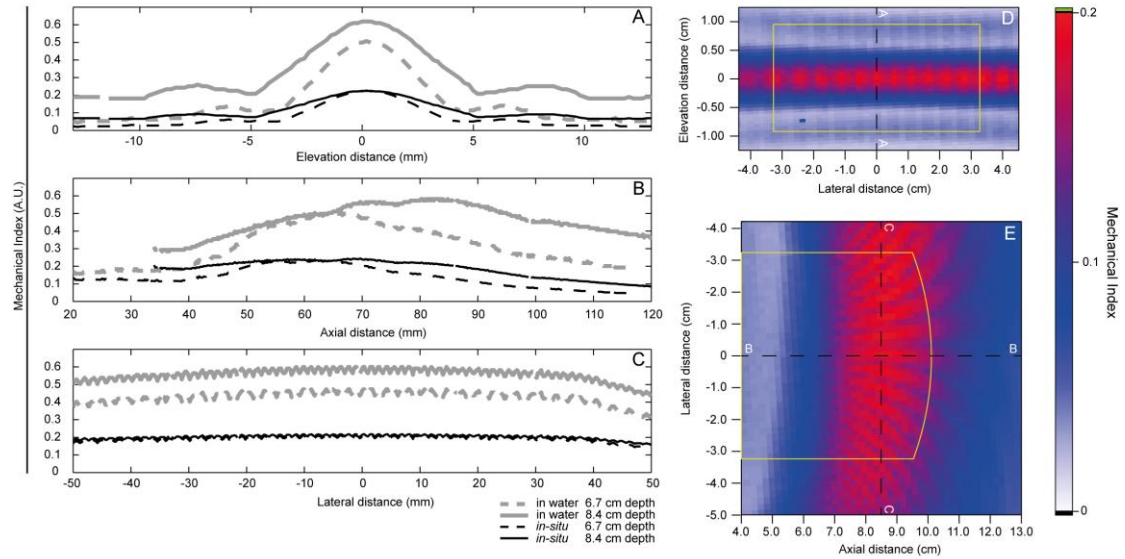


**Figure 1:** 1D and 2D beam profiles at sonoporation settings using the 4C probe at two focal depths: 6.7 cm and 8.4 cm for the 1D plots and 8.4 cm for the 2D plots. The beam profile was characterised in water and derated for *in-situ* values [44, 45]. Lines A-A, B-B, and C-C in panels D and E represent the position of the 1D scans shown in panels A, B and C respectively. The yellow bounding boxes in panels D and E represent the area visible on the clinical scanner screen. In the elevation direction the bounding box was defined by when a 0.5mm needle could not be distinguished on screen. The tumour was positioned at the intersection of lines B-B and C-C in frame E, and at an elevation distance of 0 mm in frame D.

The beam profile showed formation of multiple foci in close proximity along the lateral direction merging to form a quasi-continuous focus (Figure 1E). In the elevation direction side lobes can be clearly seen (Figure 1A and 1D). Using the full width half maximum (FWHM) to define the beam size, the active or treatment area can be defined as a volume of  $69 \times >100 \times 1.0 \text{ (mm)}^3$  ( $l \times w \times h$ ). It is assumed that this is the region where sonoporation occurred most efficiently. Figure 2 shows the pulse

169 repetition pattern generated by these settings. The pulse was amplitude-modulated,  
170 consisting of 5 cycles ( $2.1\ \mu\text{s}$ ) every  $210\ \mu\text{s}$  corresponding to a 1% duty cycle  
171 (repetition rate optimised). The duty cycle is defined as the percentage of time that  
172 ultrasound is being generated. This was measured during the spatial calibration  
173 process, in the acoustic focus with the hydrophone, for the duration of the inverse of  
174 the frame rate. Due to synthetic aperture and contrast enhanced imaging the pulse  
175 pattern at the focus was amplitude-modulated [46] [47]. This can be seen in the upper  
176 panel of Fig. 2. The lower panel of Fig. 2 shows the time signal of a single pulse. The  
177 pulse is still relatively sine-shaped, thus the transfer function of the propagation path  
178 is linear. Minor nonlinear effects can be seen after the 4<sup>th</sup> cycle. This indicates that  
179 shockwave occurrence and therefore microbubble destruction is negligible.

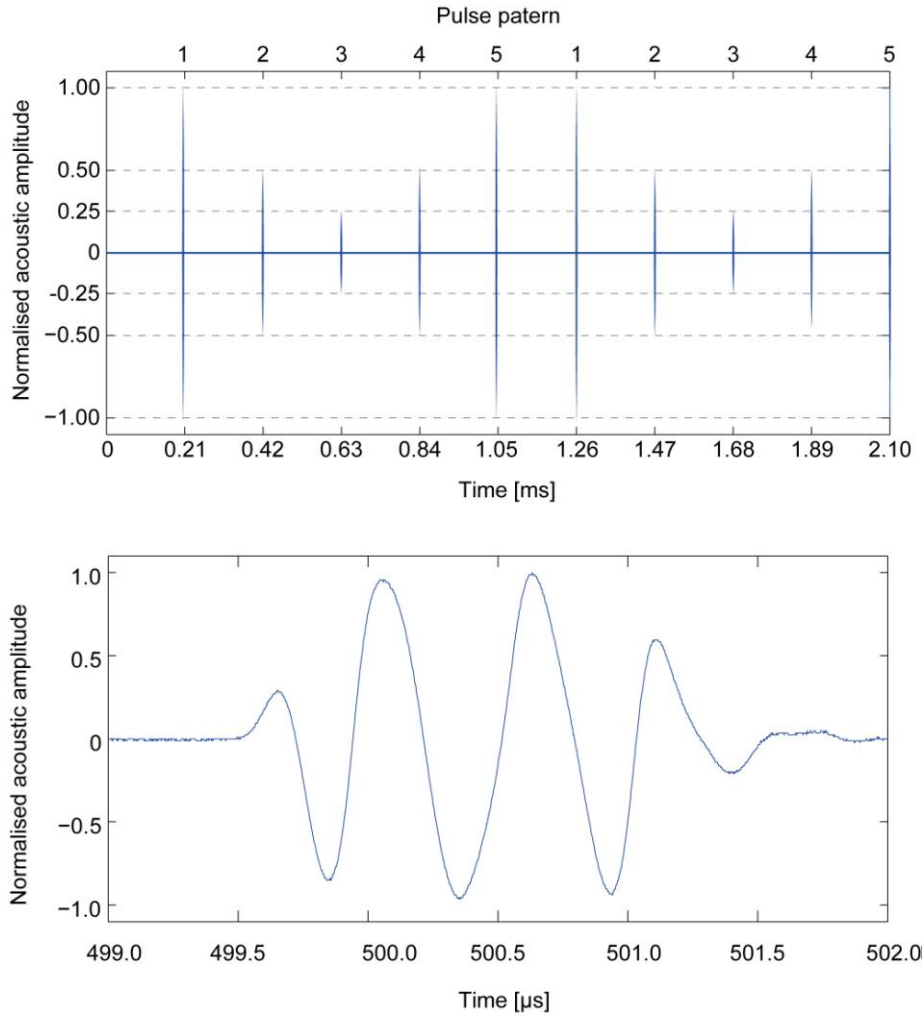


**Figure 2:** Ultrasonic pulse generated by the clinical scanner. The top panel shows the pulse repetition frequency and pattern. The lower panel shows the temporal extent of the pulse with the largest amplitude. The pulses were amplitude-modulated. Each pulse consisted of 4 cycles (2.1  $\mu$ s) every 210  $\mu$ s.

A Fast Fourier Transform (FFT) of the acoustic signal is shown in Fig. 3. The centre frequency is 1.9 MHz. Using a  $-3$ -dB or FWHM cut-off the bandwidth was measured to be 1.1 MHz; from 1.3 – 2.4 MHz. A second harmonic peak can be seen at 3.6 MHz due to the minor non-linear effects. This peak was 11 dB lower than the primary peak.

These settings complied with current safety guidelines for clinical diagnostic imaging [44, 48, 49]. Figure 4 shows two images of pancreatic cancer in two separate patients captured using the sonoporation treatment settings.

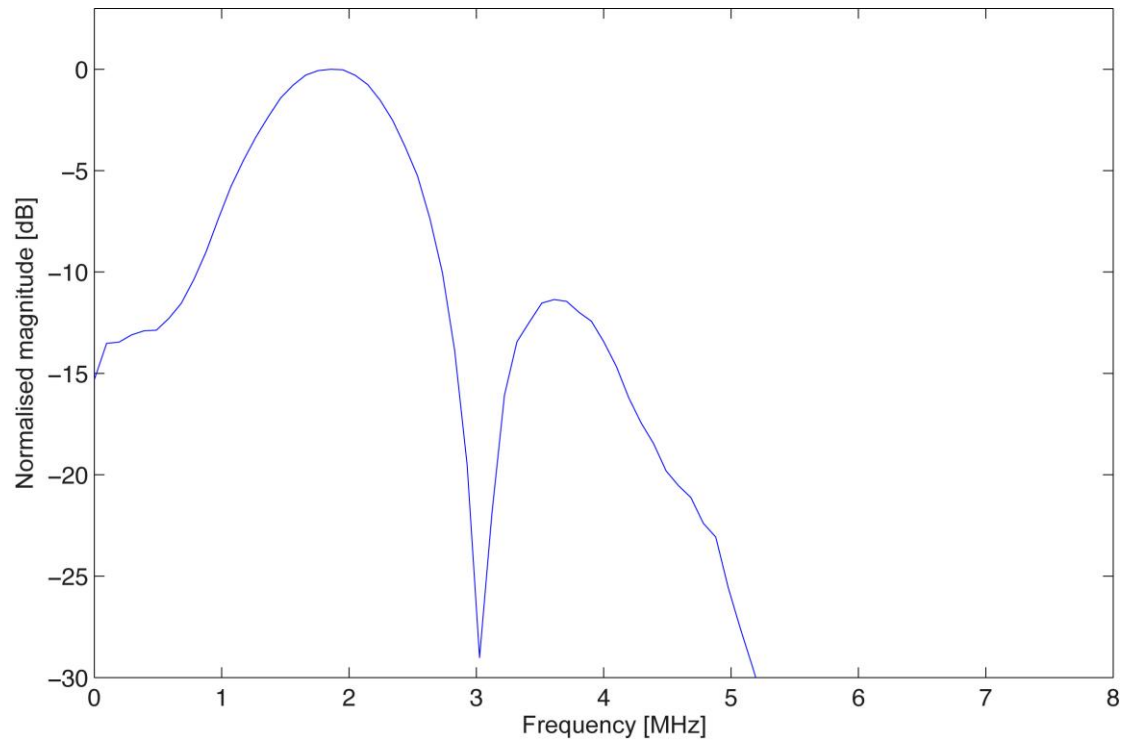


**Figure 3:** Fast Fourier transform of ultrasonic signal. The centre frequency of the transmitted signal is 1.9 MHz. A bandwidth of 1.1 MHz can be seen.

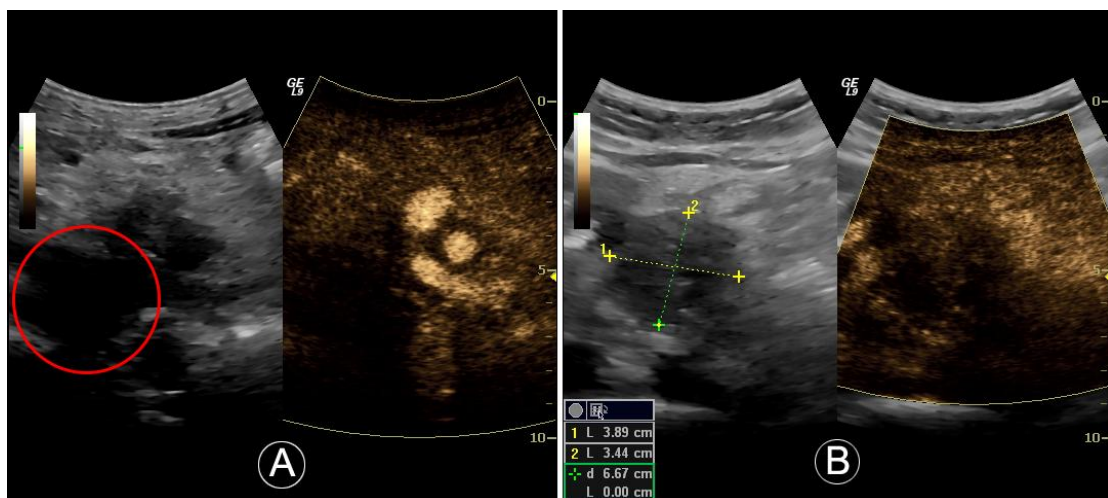


**Figure 4:** Images captured using customised sonoporation settings using a clinical ultrasound scanner. The dense vasculature in early arterial phase to the right of the main tumour (circled in red) can be seen in panel A. Panel B shows the dimensions of the main tumour, indicated by lines 1 and 2, using the sonoporation settings.

#### **Chemotherapeutic and Microbubble dosage**

The recommended chemotherapeutic protocol was followed [50]. This protocol dictates which patients are eligible for chemotherapy and the dosages that can be administered. It includes dosage reduction values depending on platelet and absolute granulocyte count. The chemotherapeutic used, gemcitabine (Gemzar<sup>®</sup>, Eli Lilly and Company, Indianapolis, IN) was administered once weekly for up to 7 weeks (or until toxicity necessitates reducing or holding a dose), followed by a week of rest from treatment. Subsequent cycles consisted of infusions once weekly for 3 consecutive weeks out of every 4 weeks. Our protocol used the Eastern Cooperative Oncology Group (ECOG) performance status as a measure of the clinical condition [51]. The ECOG performance status ranges from 0–5, where 0 denotes a “*fully active patient able to carry on all pre-disease performance without restriction*”, and 5 denotes a “*dead*” patient. Chemotherapy was halted if the patient exceeded a grade of 2 that states the patient is “*ambulatory and capable of all self-care but unable to carry out any works activities. Up and about more than 50% of waking hours.*” The ECOG guidelines can be considered as a measure of how “healthy” a patient is. We used the ECOG guidelines to monitor the effectiveness of the combined treatment *i.e.*, the longer a patient stays below an ECOG grade of 3, the more effective the treatment is considered.

A single treatment cycle is defined as a single infusion of chemotherapeutic followed by ultrasound and microbubble treatment. The week pause was not counted as a treatment cycle. Once the granulocyte or platelet count was permanently too low, or the patient surpassed an ECOG performance status grade of 2, no more treatment was administered.

Gemcitabine was administered by intravenous infusion at a dose of  $1000 \text{ mg/m}^2$  over 30 minutes. The start of the chemotherapeutic delivery is defined as  $T = 0 \text{ min}$ . During the last 10 minutes ( $T = 20 \text{ min}$ ) of chemotherapeutic delivery, diagnostic imaging was performed in standard abdominal imaging mode and the tumour was located. Here the tumour dimensions were measured with ultrasonography. Once the tumour was located, a custom made clamp was used to lock the probe in position and the clinical scanner was switched to therapeutic settings (Fig 5). As the maximum systemic concentration of the chemotherapeutic starts at the finish of delivery ( $T = 30 \text{ min}$ ) this was chosen as the initiation point for the ultrasound treatment. Clinically approved SonoVue<sup>®</sup> (Bracco Imaging Scandinavia AB, Oslo, Norway) ultrasound contrast agent was used as the microbubble for sonoporation. To ensure microbubbles were present throughout the whole treatment 0.5 mL of contrast agent followed by 5 mL saline were injected every 3.5 min, *i.e.*, at  $T = 30.0, 33.5, 37.0, 40.5, 44.0, 47.5, 51.0, 54.5$  and  $58.0 \text{ min}$ . A single vial (4.5 mL) was used throughout each treatment. Treatment was stopped at  $T = 61.5 \text{ min}$ . The total cumulated ultrasound treatment time was only 18.9 s. This time frame can be seen in Fig. 5A.

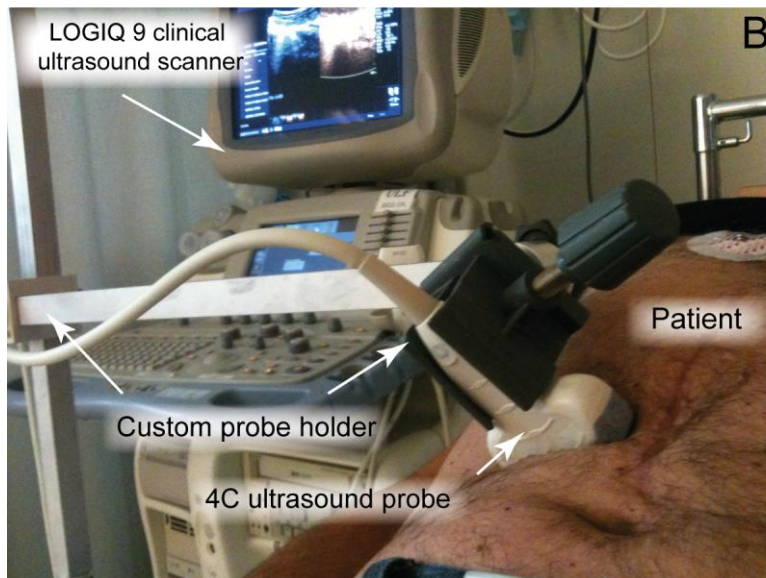
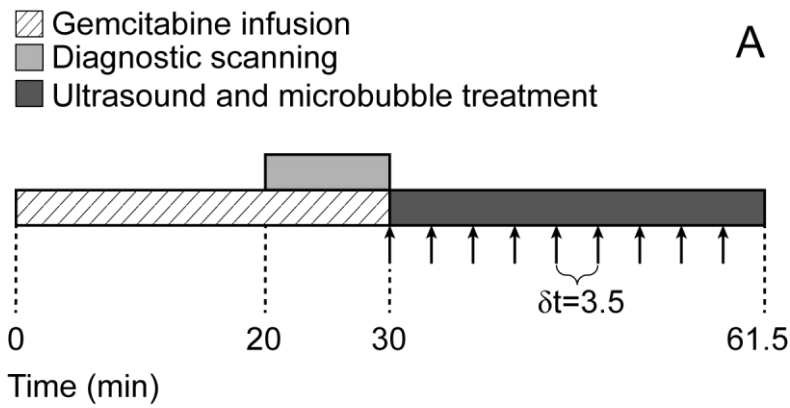


**Figure 5:** Time frame of each chemotherapy cycle (Panel A) and photograph of probe and custom made probe holder during patient treatment using microbubble sonoporation for pancreatic cancer (Panel B). Panel A shows the time frame for each treatment cycle from the start of the gemcitabine infusion. Arrows indicate intravenous injection time of 0.5 mL SonoVue<sup>®</sup> followed by a 5-mL intravenous injection of saline. Time between each injection ( $\delta t$ ) is 3.5 minutes.

## Measurement of disease and tumour progression



The primary measure for evaluating the effectiveness of the treatment was the amount of cycles the patient could undergo. The more treatment cycles the patient underwent, the longer the patient was considered healthy [50, 51]. Furthermore, if the tumour size was reduced substantially in accordance to the Response Evaluation Criteria in Solid Tumours (RECIST) [52], the treatment modality was re-evaluated, *e.g.* transfer to radiation therapy or surgery. This was considered a successful treatment.

Diagnostic ultrasound imaging was performed weekly assessing the tumour size. As Computerised Tomography CT scans are considered the golden standard for following tumour growth [53], every 8 weeks a CT scan was also performed to validate the tumour size. This value was used to follow the tumour progression.

Positron Emission Tomography (PET) imaging was also performed at the start of the treatment to assess the presence of metastasis.

Figure 6 shows the pancreatic adenocarcinoma in patient 5 prior to ultrasound and microbubble treatment as seen by CT and PET imaging modalities.

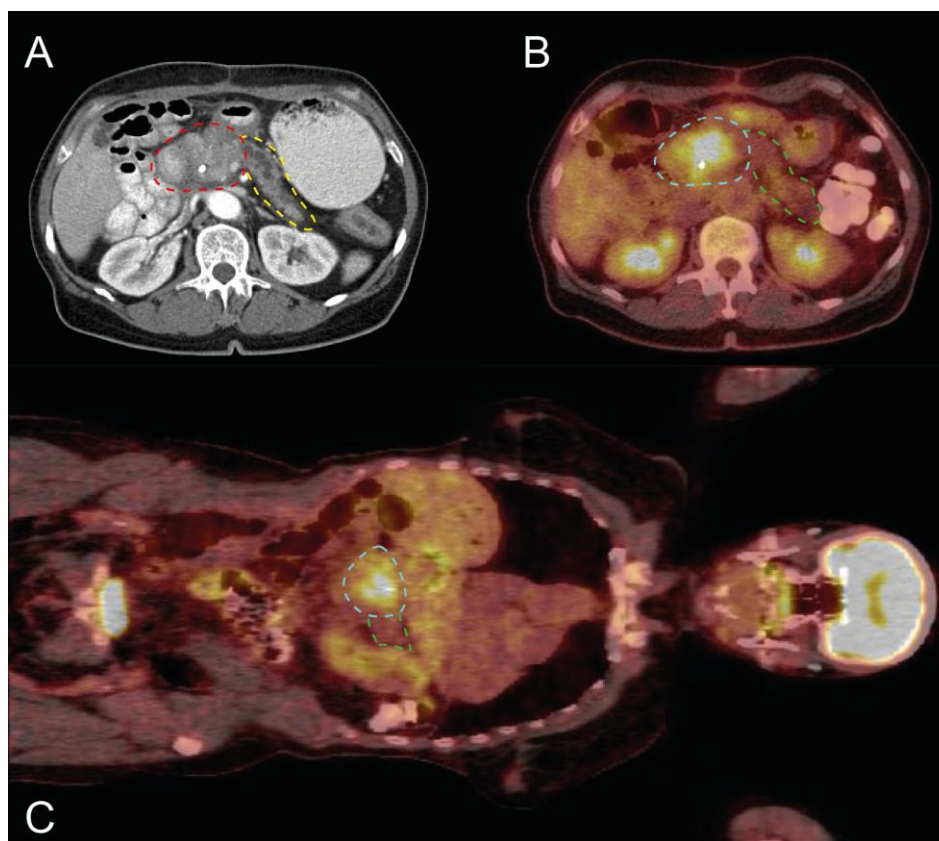


**Figure 6.** CT (Panel A) and PET (Panels B and C) images of patient 5 showing pancreatic adenocarcinoma prior to treatment. Panel A shows a CT scan in the transverse plane with the primary tumour in the head of the pancreas, and the pancreas indicated by the red and yellow dashed lines respectively. Panels B and C show PET scans in transverse and coronal plane respectively. The location of the tumour can be clearly identified by the brighter colour in the middle of the abdomen. In Panels B and C, the tumour and pancreas are respectively indicated by the blue and green dashed lines. The pancreas tail is behind the large colon in panel C.

274

## 275 **Treatment group**

276 Patients with inoperable pancreatic cancer and fulfilled the inclusion criteria at the  
 277 Haukeland University Hospital, Bergen, Norway, who have volunteered to participate,  
 278 were included. The inclusion criteria primarily stated that the patients must be > 18

years of age, a diagnosis of inoperable pancreatic cancer, histologically verified, locally advanced (stage II/III) or metastatic (stage IV) adenocarcinoma of the pancreas, and must be ambulatory with an ECOG performance status between 0 and 2. For this case report a total of five patients were recruited. Table 3 shows the characteristics of the five patients enrolled in this pilot study prior to treatment in addition to the start and end dates of the treatment for every patient.

			Patient 1	Patient 2	Patient 3	Patient 4	Patient 5
<b>Age</b>			66	55	70	68	51
<b>Sex</b>			Male	Male	Female	Female	Female
<b>Pathology Findings</b>			Pancreatic ductal adenocarcinoma				
<b>ECOG Performance</b>			0	1	1	0	1
<b>Biochemistry</b>	ALAT	IU/L	20	55	138	23	66
	LD	IU/L	121	146	153	117	176
	Leuk	$\times 10^9$ U/L	6.8	3.8	6.9	6.1	11.1
	Neutr	$\times 10^9$ U/L	4.3	5.8	3.8	3.5	7.1
<b>Tumour Markers</b>	Ca 125		ND	54.1	102	ND	136.6
	Ca 19-9		59	ND	ND	4608	ND
<b>Treatment dates (dd/mm/yyyy)</b>	Start date		06/01/2012	04/04/2012	07/03/2012	22/02/2012	15/02/2012
	End date		26/09/2012	01/08/2012	11/07/2012	11/05/2012	08/06/2012

**Table 3:** Patient characteristics prior to treatment. ND denotes non-discernable values. Start and end date of treatment are also stated.

### Control group

Taking into account the guidelines for gemcitabine treatment, it can be deduced that the more treatment cycles the patient can undergo, the longer the patient can be considered healthy; hence the more effective the treatment. Once the patient surpasses a Level 2 in the ECOG performance status guidelines, they would no longer receive treatment; this would accordingly define the end of the healthy and ambulatory period. Our control group consisted of 80 patients from 2009-2011 with histology

showing pancreatic adenocarcinoma (matching the same criteria as our patients). These patients received the identical chemotherapy treatment (in accordance to Gemzar guidelines [50]) at Haukeland University Hospital, Bergen, Norway. The control treatments were also discontinued once they surpassed and ECOG performance grade of 2 or their blood counts dropped below the chemotherapy guidelines. Patients who received a different treatment were excluded from the control group. The data was accessed through the internal hospital medical system. The same anonymous data will be available on the Norwegian national cancer registry.

## **Ethical Considerations**

All experiments were performed with approval from the regional ethics committee under reference number 2011/1601/REK vest.

## **Results and discussion**

The beam characterisation showed that the clinical scanner took into account the attenuation of soft tissue when varying the focal depth. This allowed for a good prediction of the ultrasound profile *in-situ* and easy manipulation of the ultrasound intensity and positioning. The “active” area that we assume enhances the chemotherapy effect was long and wide in all cases independent of depth, surpassing the tumour size, allowing a maximum flexibility on treatment area. It has be assumed that there are some fluctuations in the sound field pressures due to tissue property variations, but this should not drastically change the sound field in our case, as acoustic propagation was only though soft tissue. Taking into account the vast range of ultrasound intensities used to induce sonoporation, as seen in literature, we assume

that sonoporation may be occurring at lower or higher acoustic pressures independent of the varying attenuation of tissue. A benefit of using a clinical probe is also that due to the synthetic aperture, objects obscuring the field of view do not affect the beam formation in other areas; hence we can predict the ultrasound dose delivered to our target area.

The image generated using our customised treatment settings allowed easy identification of both microbubbles and tumours. Figure 4A shows clear signs of microbubble presence in the tumour vasculature and surrounding tissue. Figure 4B shows the dimensions of a pancreatic tumour indicating the ease of detecting and aligning the probe to the tumour using the modified settings.

Figure 7 shows the normalised perfusion curve where the arrows indicate the contrast injection time, as measured by the clinical scanner during the first 13 minutes of ultrasound and microbubble treatment. A pseudo-sinusoidal perfusion curve can be seen. Throughout the whole treatment we can see that there are always microbubbles present. By using this pseudo-continuous method we can ensure that there are always microbubbles present without the added complexity of continuous infusion equipment.

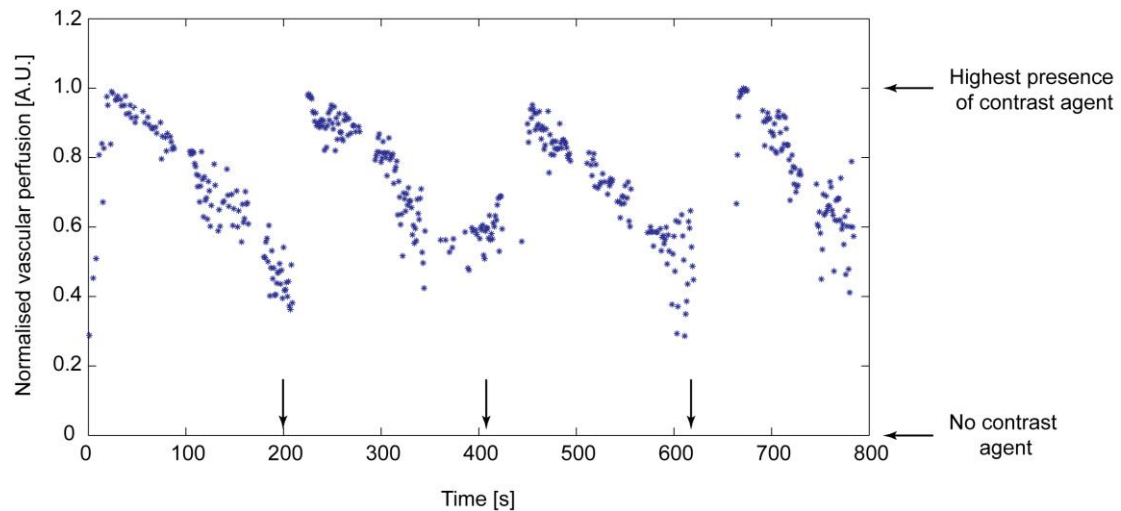


**Figure 7:** Normalised microbubble presence in tumour locality during the first 800 s of treatment. Arrows indicate contrast injection time.

Our control group, treated with the same chemotherapeutic protocol, received an average of  $9 \pm 6$  treatment cycles. To date all patients participating in this trial have already surpassed this indicating the potential benefit of our combined treatment on a clinical scale with minimal changes to chemotherapy protocols. The patients enrolled in this clinical pilot study received an average of  $16 \pm 7$  treatment cycles.

Figure 8 and Table 3 show the effect of our combined treatment on the tumour size. After 8 weeks two patients showed a tumour diameter reduction. Patient 1 had a temporary tumour reduction from 4.0 cm to 3.1 cm. The next CT image was taken 24 weeks later and showed a growth to 4.6 cm; an increase of 15% from the original tumour size after 32 weeks of treatment. In patient 2, the treatment resulted in a continuous tumour reduction over 16 weeks, a very rare response from chemotherapy alone. As a result of his increased health, after 10 treatment cycles, he was removed from the clinical trial to undergo radiation therapy. As this patient was removed from the trial due to the success of the treatment, a lower number of total and average treatments was seen, reducing the apparent effectiveness of the treatment as a whole.

It should be noted that none of the patients in the control group stopped treatment due to its success but on the contrary, due to their deterioration.

Two patients showed slow tumour growth from the 8<sup>th</sup> week onwards (patient 3 and patient 4). Patient 5 also had a biopsy verified primary tumour in the pancreas. This was surgically removed but re-occurred with a small tumour in the operation sight and a large metastasis. This indicated that the tumour was at a late stage of development hence a limited response could be expected from the chemotherapeutic. Nevertheless, this patient was also able to receive 11 cycles of treatment.

As pancreatic cancer is such an aggressive form of cancer it is very uncommon to see any decrease in tumour growth from chemotherapy. Our aim was to improve quality of life, to extend the healthy period of life, and conclusively extend the patients survival. If the patient was “healthy” enough (well-defined state in both groups, ECOG performance status 0-2 [51]), they would be able to receive treatment for a longer period. In fact, as long they are ambulatory and capable of all self-care they are able to receive the treatment. Seeing a decrease in the primary tumour size was an added benefit to the increased number of treatment cycles and thereby the anticipated survival.

Patient	Maximum tumour diameter (cm)					Total number of cycles
	Inclusion day	Week 8	Week 16	Week 24	Week 32	
1	4.0	3.1	-	-	4.6	27
2	4.9	3.9	3.6	-	-	10
3	1.5	3.0	3.5	-	-	11
4	2.2	-	2.3	2.9	3.4	16
5	4.0	-	5.5	6.2	-	16

**Table 4:** Maximum tumour diameter as measured from CT images. Empty values denote skipped CT scans.

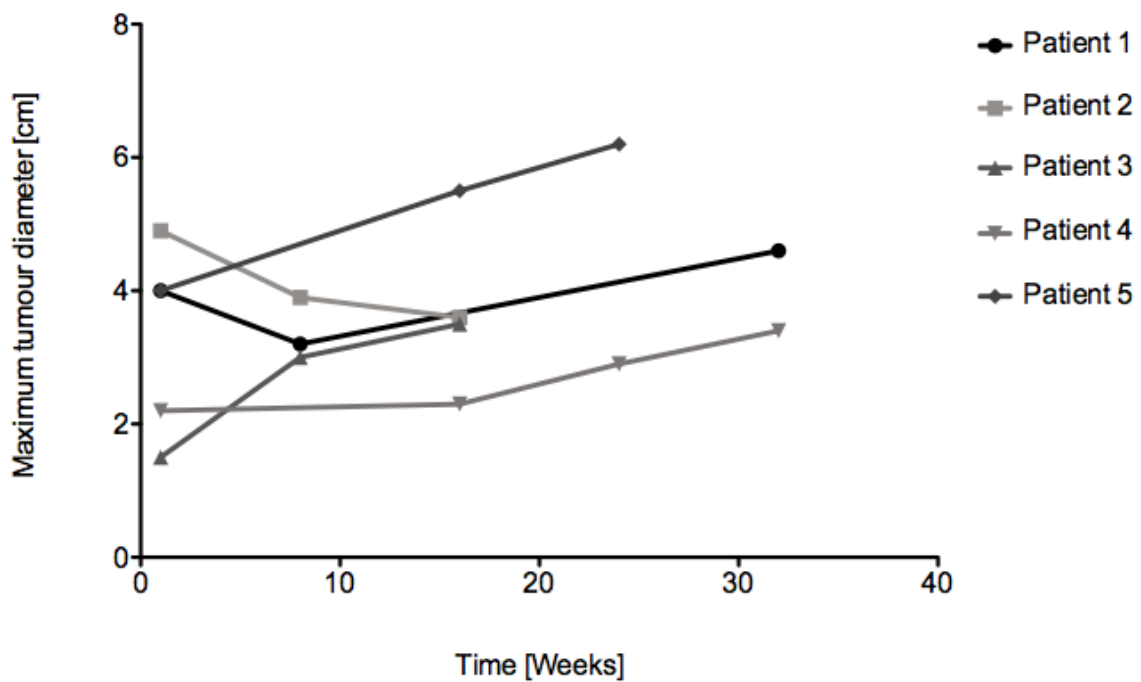


**Figure 8:** Change in tumour diameter over time measured from CT images in patients with pancreatic malignancy.



The addition of the sonoporation procedure following the standard chemotherapeutic protocol did not add any discomfort to the patients. All patients were very relaxed during the treatment to a state where they could comfortably sleep throughout the whole treatment.

In this study we also aimed to show that it is possible to induce sonoporation in the clinic using existing commercial equipment, whilst fitting in the current safety regulations for the use of diagnostic ultrasound. In our previous work we showed that a duty cycle of 40% was ideal for sonoporation [7, 23]. Here we are using a duty cycle of 1%; hence expecting a small effect of sonoporation. There are many ways to improve this method of therapy such as by increasing the duty cycle from 1% to 40% and introducing targeted microbubbles that could attach to specific cancer cells [40].

The efficacy of our combined treatment should be compared to the efficacy of the current golden standard, the chemotherapeutic gemcitabine alone, where the viability of the patient has been extended by approximately 1 month [3, 4].

## **Conclusion**

Using a clinical diagnostic scanner for therapeutic purposes allows accurate acoustic field alignment ensuring that the desired ultrasound dose reaches the target area. This configuration allows simultaneous visualisation of the microbubbles present whilst treating the pancreatic tumour. In this pilot study, we saw an extended treatment period when comparing to the control group. Furthermore, we did not notice any adverse side effects. Combined ultrasound, microbubble and chemotherapeutic treatment could pave the way for a novel enhanced drug delivery pathways.

412

## 413 **Acknowledgements**

414 This study has been supported by funds from the Norwegian Cancer Society (NCS)  
415 and MedViz (<http://medviz.uib.no/>), an interdisciplinary research cluster from  
416 Haukeland University Hospital, University of Bergen and Christian Michelsen  
417 Research AS. We would like to thank Dr. Martin Biermann, Dr. Tormod Bjårnnes, Dr.  
418 Bjørn Tore Gjertsen, Dr. Anders Molven and Dr. Halfdan Sørbye for their support  
419 throughout this project.

420

421

## 422 References

423

- 424 [1] World Health Organization. (2012). *World Health Statistics*. Available:  
425 [http://www.who.int/gho/publications/world\\_health\\_statistics/2012/en/index.ht](http://www.who.int/gho/publications/world_health_statistics/2012/en/index.html)  
426 [ml](http://www.who.int/gho/publications/world_health_statistics/2012/en/index.html)
- 427 [2] D. Hariharan, A. Saied, and H. M. Kocher, "Analysis of mortality rates for  
428 pancreatic cancer across the world," *HPB (Oxford)*, vol. **10**, pp. 58-62, (2008).
- 429 [3] J. P. Neoptolemos, J. A. Dunn, D. D. Stocken, J. Almond, K. Link, H. Beger,  
430 C. Bassi, M. Falconi, P. Pederzoli, C. Dervenis, L. Fernandez-Cruz, F. Lacaine,  
431 A. Pap, D. Spooner, D. J. Kerr, H. Friess, M. W. Buchler, and C. European  
432 Study Group for Pancreatic, "Adjuvant chemoradiotherapy and chemotherapy  
433 in resectable pancreatic cancer: a randomised controlled trial," *Lancet*, vol.  
434 **358**, pp. 1576-1585, (2001).
- 435 [4] J. P. Neoptolemos, D. D. Stocken, H. Friess, C. Bassi, J. A. Dunn, H. Hickey,  
436 H. Beger, L. Fernandez-Cruz, C. Dervenis, F. Lacaine, M. Falconi, P.  
437 Pederzoli, A. Pap, D. Spooner, D. J. Kerr, M. W. Buchler, and C. European  
438 Study Group for Pancreatic, "A randomized trial of chemoradiotherapy and  
439 chemotherapy after resection of pancreatic cancer," *N Engl J Med*, vol. **350**,  
440 pp. 1200-1210, (2004).
- 441 [5] S. Bao, B. D. Thrall, and D. L. Miller, "Transfection of a reporter plasmid into  
442 cultured cells by sonoporation in vitro," *Ultrasound Med. Biol.*, vol. **23**, pp.  
443 953-959, (1997).
- 444 [6] A. van Wamel, K. Kooiman, M. Harteveld, M. Emmer, F. J. ten Cate, M.  
445 Versluis, and N. de Jong, "Vibrating microbubbles poking individual cells:  
446 drug transfer into cells via sonoporation," *J. Control. Release*, vol. **112**, pp.  
447 149-155, (2006).
- 448 [7] A. Delalande, S. Kotopoulis, T. Rovers, C. Pichon, and M. Postema,  
449 "Sonoporation at a low mechanical index," *Bub. Sci. Eng. Tech.*, vol. **3**, pp. 3-  
450 11, (2011).
- 451 [8] M. Postema, S. Kotopoulis, A. Delalande, and O. H. Gilja, "Sonoporation:  
452 Why microbubbles create pores," *Ultraschall in Med.*, vol. **33**, pp. 97-98,  
453 (2012).
- 454 [9] N. G. Lee, J. L. Berry, T. C. Lee, A. T. Wang, S. Honowitz, A. L. Murphree,  
455 N. Varshney, D. R. Hinton, and A. A. Fawzi, "Sonoporation enhances  
456 chemotherapeutic efficacy in retinoblastoma cells in vitro," *Invest Ophthalmol*  
457 *Vis Sci*, vol. **52**, pp. 3868-3873, (2011).
- 458 [10] C. X. Deng, F. Sieling, H. Pan, and J. Cui, "Ultrasound-induced cell  
459 membrane porosity," *Ultrasound Med Biol*, vol. **30**, pp. 519-526, (2004).
- 460 [11] R. K. Schlicher, H. Radhakrishna, T. P. Tolentino, R. P. Apkarian, V.  
461 Zarnitsyn, and M. R. Prausnitz, "Mechanism of intracellular delivery by  
462 acoustic cavitation," *Ultrasound Med Biol*, vol. **32**, pp. 915-924, (2006).
- 463 [12] Y. Z. Zhao, Y. K. Luo, C. T. Lu, J. F. Xu, J. Tang, M. Zhang, Y. Zhang, and H.  
464 D. Liang, "Phospholipids-based microbubbles sonoporation pore size and  
465 reseal of cell membrane cultured in vitro," *J Drug Target*, vol. **16**, pp. 18-25,  
466 (2008).
- 467 [13] M. Postema and O. H. Gilja, "Ultrasound-directed drug delivery," *Curr.*  
468 *Pharm. Biotechnol.*, vol. **8**, pp. 355-361, (2007).

- 469 [14] M. Postema, O. H. Gilja, and A. van Wamel, "CEUS and sonoporation," in  
470 *Fundamentals of Medical Ultrasonics*, M. Postema, Ed., London: Spon press,  
471 2011, pp. 205-217.
- 472 [15] M. Postema, S. Kotopoulis, A. Delalande, and O. H. Gilja, "Ultrasound-guided  
473 delivery and sonoporation," in *Ultrasound in Gastroenterology. 10-years*  
474 *aniversary of National Center for Ultrasound in Gastroenterology*, 2011, pp.  
475 57-59.
- 476 [16] J. M. Escoffre, A. Novell, J. Piron, A. Zeghimi, A. Doinikov, and A. Bouakaz,  
477 "Microbubble attenuation and destruction: are they involved in sonoporation  
478 efficiency?," *IEEE Trans Ultrason Ferroelectr Freq Control*, vol. **60**, pp. 46-  
479 52, (2013).
- 480 [17] D. L. Miller and C. Dou, "Membrane damage thresholds for 1- to 10-MHz  
481 pulsed ultrasound exposure of phagocytic cells loaded with contrast agent gas  
482 bodies in vitro," *Ultrasound Med. Biol.*, vol. **30**, pp. 973-977, (2004).
- 483 [18] D. L. Miller and C. Dou, "Membrane damage thresholds for pulsed or  
484 continuous ultrasound in phagocytic cells loaded with contrast agent gas  
485 bodies," *Ultrasound Med. Biol.*, vol. **30**, pp. 405-411, (2004).
- 486 [19] D. L. Miller, C. Dou, and J. Song, "DNA transfer and cell killing in  
487 epidermoid cells by diagnostic ultrasound activation of contrast agent gas  
488 bodies in vitro," *Ultrasound Med. Biol.*, vol. **29**, pp. 601-607, (2003).
- 489 [20] D. L. Miller and J. Quddus, "Sonoporation of monolayer cells by diagnostic  
490 ultrasound activation of contrast-agent gas bodies," *Ultrasound Med. Biol.*, vol.  
491 **26**, pp. 661-667, (2000).
- 492 [21] M. W. Miller, "Gene transfection and drug delivery," *Ultrasound Med. Biol.*,  
493 vol. **26**, pp. S59-S62, (2000).
- 494 [22] K. Kooiman, M. Harteveld, A. F. W. van der Steen, and N. de Jong,  
495 "Sonoporation of endothelial cells by vibrating targeted microbubbles," *J.*  
496 *Control Release*, vol. **154**, pp. 35-41, (2011).
- 497 [23] A. Delalande, A. Bouakaz, G. Renault, F. Tabareau, S. Kotopoulis, P. Midoux,  
498 B. Arbeille, R. Uzbekov, S. Chakravarti, M. Postema, and C. Pichon,  
499 "Ultrasound and microbubble-assisted gene delivery in Achilles tendons: long  
500 lasting gene expression and restoration of fibromodulin KO phenotype," *J*  
501 *Control Release*, vol. **156**, pp. 223-230, (2011).
- 502 [24] S. M. Nejad, S. H. R. Hosseini, H. Akiyama, and K. Tachibana, "Optical  
503 observation of cell sonoporation with low intensity ultrasound," *Biochemical*  
504 *and Biophysical Research Communications*, vol. **413**, pp. 218-223, (2011).
- 505 [25] F. Yang, N. Gu, D. Chen, X. Xi, D. Zhang, Y. Li, and J. Wu, "Experimental  
506 study on cell self-sealing during sonoporation," *J Control Release*, vol. **131**,  
507 pp. 205-210, (2008).
- 508 [26] Y. Qiu, C. Zhang, J. Tu, and D. Zhang, "Microbubble-induced sonoporation  
509 involved in ultrasound-mediated DNA transfection in vitro at low acoustic  
510 pressures," *Journal of Biomechanics*, vol. **45**, pp. 1339-1345, (2012).
- 511 [27] M. Matsuo, K. Yamaguchi, L. B. Feril, Jr., H. Endo, K. Ogawa, K. Tachibana,  
512 and J. Nakayama, "Synergistic inhibition of malignant melanoma proliferation  
513 by melphalan combined with ultrasound and microbubbles," *Ultrason*  
514 *Sonochem*, vol. **18**, pp. 1218-1224, (2011).
- 515 [28] N. Lamanauskas, A. Novell, J. M. Escoffre, M. Venslauskas, S. Satkauskas,  
516 and A. Bouakaz, "Bleomycin delivery into cancer cells in vitro with  
517 ultrasound and SonoVue® or BR14® microbubbles.," *J Drug Target*, vol. **1**, p.  
518 [Epub ahead of print], (2013).

- 519 [29] Y. Watanabe, A. Aoi, S. Horie, N. Tomita, S. Mori, H. Morikawa, Y.  
520 Matsumura, G. Vassaux, and T. Kodama, "Low-intensity ultrasound and  
521 microbubbles enhance the antitumor effect of cisplatin," *Cancer Sci*, vol. **99**,  
522 pp. 2525-2531, (2008).
- 523 [30] J. Wu, J. Pepe, and M. Rincon, "Sonoporation, anti-cancer drug and antibody  
524 delivery using ultrasound," *Ultrasonics*, vol. **44**, pp. E21-E25, (2006).
- 525 [31] C. Y. Lai, C. H. Wu, C. C.C., and P. C. Li, "Quantitative relations of acoustic  
526 inertial cavitation with sonoporation and cell viability," *Ultrasound Med. Biol.*,  
527 vol. **32**, pp. 1931-1941, (2006).
- 528 [32] D. M. Hallow, A. D. Mahajan, T. E. McCutchen, and M. R. Prausnitz,  
529 "Measurement and correlation of acoustic cavitation with cellular bioeffects,"  
530 *Ultrasound Med. Biol.*, vol. **32**, pp. 1111-1122, (2006).
- 531 [33] M. M. Forbes, R. L. Steinberg, and W. D. O'Brien, "Examination of Inertial  
532 Cavitation of Optison in Producing Sonoporation of Chinese Hamster Ovary  
533 Cells," *Ultrasound in Medicine and Biology*, vol. **34**, pp. 2009-2018, (2008).
- 534 [34] J. L. Tlaxca, C. R. Anderson, A. L. Klibanov, B. Lowrey, J. A. Hossack, J. S.  
535 Alexander, M. B. Lawrence, and J. J. Rychak, "Analysis of in vitro  
536 Transfection by Sonoporation Using Cationic and Neutral Microbubbles,"  
537 *Ultrasound Med Biol*, vol. **36**, pp. 1907-1918, (2010).
- 538 [35] C. D. Ohl and B. Wolfrum, "Detachment and sonoporation of adherent HeLa-  
539 cells by shock wave-induced cavitation," *Biochimica Et Biophysica Acta-  
540 General Subjects*, vol. **1624**, pp. 131-138, (2003).
- 541 [36] D. L. Miller and C. Y. Dou, "Induction of Apoptosis in Sonoporation and  
542 Ultrasonic Gene Transfer," *Ultrasound in Medicine and Biology*, vol. **35**, pp.  
543 144-154, (2009).
- 544 [37] M. Postema and O. H. Gilja, "Jetting does not cause sonoporation," *Biomed.  
545 Eng.*, vol. **55**, pp. S19-S20, (2010).
- 546 [38] B. Geers, H. Dewitte, S. C. De Smedt, and I. Lentacker, "Crucial factors and  
547 emerging concepts in ultrasound-triggered drug delivery," *J Control Release*,  
548 vol. **164**, pp. 248-255, (2012).
- 549 [39] F. G. Erchinger, G. Dimceviski, T. Engjom, and O. H. Gilja, "Transabdominal  
550 ultrasonography of the pancreas: basic and new aspects," *Imaging Med.*, vol. **3**,  
551 pp. 412-422, (2011).
- 552 [40] M. Postema and O. H. Gilja, "Contrast-enhanced and targeted ultrasound,"  
553 *World J. Gastroenterol.*, vol. **17**, pp. 28-41, (2011).
- 554 [41] F. Piscaglia, C. Nolsoe, C. F. Dietrich, D. O. Cosgrove, O. H. Gilja, M.  
555 Bachmann Nielsen, T. Albrecht, L. Barozzi, M. Bertolotto, O. Catalano, M.  
556 Claudon, D. A. Clevert, J. M. Correas, M. D'Onofrio, F. M. Drudi, J. Eyding,  
557 M. Giovannini, M. Hocke, A. Ignee, E. M. Jung, A. S. Klausner, N. Lassau, E.  
558 Leen, G. Mathis, A. Saftoiu, G. Seidel, P. S. Sidhu, G. ter Haar, D.  
559 Timmerman, and H. P. Weskott, "The EFSUMB Guidelines and  
560 Recommendations on the Clinical Practice of Contrast Enhanced Ultrasound  
561 (CEUS): update 2011 on non-hepatic applications," *Ultraschall in Med.*, vol.  
562 **33**, pp. 33-59, (2012).
- 563 [42] M. Postema, *Fundamentals of medical ultrasonics*. Milton Park, Abingdon,  
564 Oxon ; New York: Spon Press, 2011.
- 565 [43] B. Gerold, S. Kotopoulis, M. C., D. McGloin, M. Postema, and P. Prentice,  
566 "Laser-nucleated acoustic cavitation in focused ultrasound," *Rev. Sci. Instrum.*,  
567 vol. **82**, p. 044908, (2011).

- [44] U.S. Department of Health and Human Services. Food and Drug Administration, "Information for Manufacturers Seeking Marketing Clearance of Diagnostic Ultrasound Systems and Transducers," 2008.
- [45] International Electrotechnical Commission, "Ultrasonics - Hydrophones - Part 2: Calibration for ultrasonic fields up to 40 MHz," 2013.
- [46] J. A. Jensen, S. I. Nikolov, K. L. Gammelmark, and M. H. Pedersen, "Synthetic aperture ultrasound imaging," *Ultrasonics*, vol. **44 Suppl 1**, pp. e5-15, (2006).
- [47] E. Quaia, "Microbubble ultrasound contrast agents: an update," *European Radiology*, vol. **17**, pp. 1995-2008, (2007).
- [48] British Medical Ultrasound Society, *Guidelines for the safe use of diagnostic ultrasound equipment*, 2000.
- [49] S. B. Barnett, G. R. Ter Haar, M. C. Ziskin, H. D. Rott, F. A. Duck, and K. Maeda, "International recommendations and guidelines for the safe use of diagnostic ultrasound in medicine," *Ultrasound Med Biol*, vol. **26**, pp. 355-366, (2000).
- [50] Eli Lilly and Company. (2010). *Highlights of prescribing information - Gemzar*. Available: <http://pi.lilly.com/us/gemzar.pdf>
- [51] M. M. Oken, R. H. Creech, D. C. Tormey, J. Horton, T. E. Davis, E. T. Mcfadden, and P. P. Carbone, "Toxicity and Response Criteria of the Eastern-Cooperative-Oncology-Group," *American Journal of Clinical Oncology-Cancer Clinical Trials*, vol. **5**, pp. 649-655, (1982).
- [52] E. A. Eisenhauer, P. Therasse, J. Bogaerts, L. H. Schwartz, D. Sargent, R. Ford, J. Dancey, S. Arbuck, S. Gwyther, M. Mooney, L. Rubinstein, L. Shankar, L. Dodd, R. Kaplan, D. Lacombe, and J. Verweij, "New response evaluation criteria in solid tumours: Revised RECIST guideline (version 1.1)," *European Journal of Cancer*, vol. **45**, pp. 228-247, (2009).
- [53] S. A. Sohaib, B. Turner, J. A. Hanson, M. Farquharson, R. T. Oliver, and R. H. Reznek, "CT assessment of tumour response to treatment: comparison of linear, cross-sectional and volumetric measures of tumour size," *Br J Radiol*, vol. **73**, pp. 1178-1184, (2000).